



**HAL**  
open science

## Impaired Activated/Memory Regulatory T Cell Clonal Expansion Instigates Diabetes in NOD Mice

Vanessa Mhanna, Gwladys Fourcade, Pierre Barennes, Valentin Quiniou, Hang P Pham, Paul-Gydeon Ritvo, Faustine Brimaud, Bruno Gouritin, Guillaume Churlaud, Adrien Six, et al.

► **To cite this version:**

Vanessa Mhanna, Gwladys Fourcade, Pierre Barennes, Valentin Quiniou, Hang P Pham, et al.. Impaired Activated/Memory Regulatory T Cell Clonal Expansion Instigates Diabetes in NOD Mice. *Diabetes*, 2021, 70 (4), pp.976-985. 10.2337/db20-0896 . hal-03263428

**HAL Id: hal-03263428**

**<https://hal.sorbonne-universite.fr/hal-03263428>**

Submitted on 17 Jun 2021

**HAL** is a multi-disciplinary open access archive for the deposit and dissemination of scientific research documents, whether they are published or not. The documents may come from teaching and research institutions in France or abroad, or from public or private research centers.

L'archive ouverte pluridisciplinaire **HAL**, est destinée au dépôt et à la diffusion de documents scientifiques de niveau recherche, publiés ou non, émanant des établissements d'enseignement et de recherche français ou étrangers, des laboratoires publics ou privés.

1 **Impaired activated/memory regulatory T cell clonal expansion instigates**  
2 **diabetes in NOD mice**

3

4 Vanessa Mhanna<sup>a</sup>, Gwladys Fourcade<sup>a</sup>, Pierre Barennes<sup>a</sup>, Valentin Quiniou<sup>a,b</sup>, Hang P.  
5 Pham<sup>c</sup>, Paul-Gydeon Ritvo<sup>a</sup>, Faustine Brimaud<sup>a</sup>, Bruno Gouritin<sup>a</sup>, Guillaume Churlaud<sup>a,b</sup>,  
6 Adrien Six<sup>a,1</sup>, Encarnita Mariotti-Ferrandiz<sup>a,1</sup>, David Klatzmann<sup>a,b,1\*</sup>

7

8 <sup>a</sup>Sorbonne Université, INSERM, Immunology-Immunopathology-Immunotherapy (i3),  
9 F-75005 Paris, France.

10 <sup>b</sup>AP-HP, Hôpital Pitié-Salpêtrière, Biotherapy (CIC-BTi) and  
11 Inflammation-Immunopathology-Biotherapy Department (i2B), F-75013, Paris, France.

12 <sup>c</sup>ILTOO Pharma, Statistics Department, Paris, France.

13 <sup>1</sup>co-senior authors

14 \*corresponding author

15 **Email:** [david.klatzmann@sorbonne-universite.fr](mailto:david.klatzmann@sorbonne-universite.fr)

16 **Phone number:** +33 1 42 17 74 60

17

18 **Word count:** 3994

19 **Number of figures:** 5

20 **Keywords**

21 Tolerance, immune regulation, immunopathology, immunotherapy, systems biology

22

23 **Abstract**

24 Regulatory T cell (Treg) insufficiency licenses the destruction of insulin-producing  
25 pancreatic  $\beta$  cells by auto-reactive effector T cells (Teffs), causing spontaneous  
26 autoimmune diabetes in non-obese diabetic (NOD) mice. We investigated the  
27 contribution to diabetes of the TCR repertoires of naive regulatory T cells (nTregs),  
28 activated/memory Tregs (amTregs), and  $CD4^+$  Teffs from prediabetic NOD mice and  
29 normal C57BL/6 (B6) mice. NOD mice amTreg and Teff repertoire diversity was  
30 unexpectedly higher than that of B6 mice. This was due to the presence of highly  
31 expanded clonotypes in B6 amTregs and Teffs that were largely lost in their NOD  
32 counterparts. IL-2 administration to NOD mice restored such amTreg clonotype  
33 expansions and prevented diabetes development. In contrast, IL-2 administration only led  
34 to few or no clonotype expansions in nTregs and Teffs, respectively. Noteworthy, IL-2  
35 expanded amTreg and nTreg clonotypes were markedly enriched in islet-antigen specific  
36 TCRs. Altogether, our results highlight the link between a reduced clonotype expansion  
37 within the activated Treg repertoire and the development of an autoimmune disease. They  
38 also indicate that the repertoire of amTregs is amenable to rejuvenation by IL-2.

39 Non-obese diabetic (NOD) mice spontaneously develop autoimmune diabetes due to the  
40 destruction of insulin-producing  $\beta$  cells by auto-reactive CD4<sup>+</sup> and CD8<sup>+</sup> T cells (1).  
41 Diabetes susceptibility in NOD mice is attributed to genetic defects encoded by the  
42 insulin-dependent diabetes (idd) loci including over 40 genes, among which the MHC  
43 class II and interleukin-2 (IL-2) genes have major contributions to the pathophysiological  
44 immune response leading to diabetes (2). The unique I-A<sup>g7</sup> MHC-II molecule expressed  
45 by NOD mice has been reported to bind certain peptides with low affinity, thus impairing  
46 the thymocyte negative selection process (3,4). Reduced IL-2 production by activated  
47 effector T cells (Teffs) was found in NOD mice and linked to an impairment of Treg  
48 numbers and functionality (5-7). An increased diabetes incidence was observed in NOD  
49 mice bearing an IL-2 alpha receptor subunit with reduced affinity for IL-2, which was  
50 associated with a Treg but not a Teff defect (8). Likewise, the administration of low-dose  
51 IL-2 to NOD mice promotes Treg expansion and activation, prevents diabetes onset and  
52 even cures diabetic mice (9, 10). Thus, the altered tolerance promoting diabetes in NOD  
53 mice could be the result of (i) a defect in thymic selection of Treg and Teff T-cell  
54 receptor (TCR) repertoires and/or (ii) an altered Treg fitness due to IL-2 deprivation.

55 Previous studies of the TCR repertoires of NOD mice and type 1 diabetes patients yielded  
56 inconsistent results. Some studies showed a restricted TRBV and TRBJ chain usage by  
57 CD4<sup>+</sup> T cells from pancreatic islets and pancreatic lymph nodes (PLN), indicating that  
58 overrepresented islet-specific TCRs preferentially express certain TRBVJ genes (11–13).  
59 Conversely, others showed a rather diverse gene usage among islet-infiltrating CD4<sup>+</sup> T  
60 cells in NOD mice (14), including islet-infiltrating memory CD4<sup>+</sup> T cells (15, 16), and no  
61 common highly used TRBVBJ combinations in T cells from PLN of type 1 diabetes

62 patients (17). Moreover, NOD Tregs were found to have a restricted TRA repertoire and  
63 limited overlap with thymic CD4<sup>+</sup> T cells (18, 19), while we found similar TRB diversity  
64 between NOD peripheral Tregs and Teffs (20). These somehow conflicting results can be  
65 explained by the fact that (i) most of these studies were performed on unsorted CD4<sup>+</sup> T  
66 cells and thus did not distinguish between regulatory and effector populations and/or (ii)  
67 most Treg repertoire analyses were done on a limited fraction of the repertoire by using  
68 TCR transgenic NOD mice or by focusing on few rearrangements (18, 19). More  
69 importantly, most studies have overlooked the existence of regulatory T cell subsets.  
70 Indeed, we previously showed that Tregs could be phenotypically divided into  
71 CD4<sup>+</sup>Foxp3<sup>+</sup>CD44<sup>low</sup>CD62L<sup>high</sup> naïve Tregs (nTregs) that have a low turnover, and  
72 CD4<sup>+</sup>Foxp3<sup>+</sup>CD44<sup>high</sup>CD62L<sup>low</sup> activated/memory Tregs (amTregs) that have a very  
73 rapid turnover due to their interaction with their cognate antigens (21). In the healthy B6  
74 mouse background, we showed that amTregs are enriched in deep tissue-draining lymph  
75 nodes (LNs) and are characterized by unique clonotype expansions (22). Moreover, we  
76 showed little overlap between amTreg and nTreg TRB repertoires (22). Thus, studying  
77 amTreg and nTreg TCR repertoires without separating them may be confounding.  
78 Here we compared the TCR repertoire of splenic amTregs, nTregs and Teffs of  
79 prediabetic NOD and normal B6 mice to investigate whether and how an altered TCR  
80 repertoire contributes to diabetes. We found that NOD amTregs have an unexpectedly  
81 more diverse repertoire than that of B6 mice, due to the absence of expanded clonotypes.  
82 Treatment of prediabetic NOD mice with IL-2, which prevents diabetes occurrence,  
83 restored the expansion of clonotypes that are preferentially diabetes-reactive. Thus, the

84 TCR repertoire of amTregs is altered by an IL-2 insufficiency, which instigates diabetes  
85 development in NOD mice, and is amenable to therapeutic recovery.

## 86 **Research Design and Methods**

### 87 **Study design**

88 Given the rarity of some of the studied cell subsets, we pooled the spleens of 6 to 8 young  
89 mice matched for genetic background, age and sex. Six (three female and three male)  
90 non-treated C57BL/6 or NOD pools of mice were used to study the repertoire at  
91 homeostasis. Six young female NOD mice were treated with IL-2. Sample size was  
92 determined for statistical significance and experimental feasibility. Investigators were not  
93 blinded to the allocations during experiments and analyses.

### 94 **Mice**

95 Eight- to ten-week-old male and female C57BL/6- and NOD-Foxp3-EGFP transgenic  
96 mice expressing green fluorescent protein (GFP) under the control of the Foxp3 gene  
97 promoter were respectively provided by B. Malissen (Luminy, Marseille) and V.  
98 Kuchroo (Brigham and Women's Hospital, Boston, MA). All animals were maintained at  
99 the Sorbonne Université Centre d'Expérimentation Fonctionnelle animal facility under  
100 specific pathogen-free conditions in agreement with the current European legislation on  
101 animal care, housing and scientific experimentation (agreement number A751315). All  
102 procedures were approved by the local animal ethics committee.

103 **IL-2 treatment**

104 Recombinant AAV8 vectors were produced as described previously (9). Six female  
105 NOD-Foxp3-EGFP mice were injected once intraperitoneally with  $10^{11}$  of rAAVs diluted  
106 in PBS at 6 weeks of age. Serum was collected two weeks post-injection and IL-2 levels  
107 were measured using a mouse IL-2 ELISA (eBioscience) according to the manufacturer's  
108 recommendations. Mice were sacrificed at nine weeks of age.

109 **Spleen retrieval and cell sorting**

110 Spleens were collected from euthanized mice and splenocytes were stained with anti-Ter-  
111 119-biotin (BD Biosciences), -B220-biotin (eBioscience) and -CD11c-biotin  
112 (eBioscience) antibodies for 20 min at 4°C and labeled with anti-biotin magnetic beads  
113 (Miltenyi Biotec) for 15 min at 4°C. B cells, erythrocytes and monocytes were depleted  
114 on an AutoMACS separator (Miltenyi Biotec) following the manufacturer's procedure.  
115 Enriched T cells were stained for 20 min at 4°C with the following monoclonal  
116 antibodies at predetermined optimal dilutions: CD3-APC (BD Biosciences), CD4-  
117 Horizon-V500 (BD Biosciences), CD8-Alexa-700 (BD Biosciences), CD44-PE (BD  
118 Biosciences) and CD62L-eFluor-450 (eBioscience) and sorted on a FACSAria II  
119 cytometer (BD Biosciences) with a purity > 95% into the following subsets: CD4<sup>+</sup>  
120 FoxP3<sup>+</sup> CD62<sup>low</sup> CD44<sup>high</sup> (activated/memory Tregs (amTregs)), CD4<sup>+</sup> FoxP3<sup>+</sup> CD62<sup>high</sup>  
121 CD44<sup>low</sup> (naive Tregs (nTregs)) and CD4<sup>+</sup> FoxP3<sup>-</sup> (T effector cells (Teffs)).  $1.10^5$  to  $5.10^6$   
122 sorted cells were stored in RNAqueous kit lysis buffer (Invitrogen) at -80 °C.

## 123 **cDNA library preparation for TR sequencing**

124 RNA was extracted using the RNAqueous Total RNA Isolation Kit (Invitrogen). TRB  
125 libraries were prepared on 100 ng of RNA with the SMARTer Mouse TCRA/b Profiling  
126 Kit (TakaraBio) and sequenced with HiSeq 2500 single read (300 bp) (Illumina) + 10%  
127 PhiX at the “LIGAN Genomics platform” (23).

## 128 **Raw read processing**

129 Raw data in FASTQ format were processed for TRB sequence annotation using MiXCR  
130 software (v.3.0.3) (24), which ensures PCR and sequencing error corrections and  
131 provides for each sample a list of unique amino acid TRBs and their corresponding  
132 counts. Annotated sequences were then analyzed using an in-house workflow to eliminate  
133 long amino acid CDR3 sequences (length higher than the mean + 8). The resulting  
134 datasets are summarized in Table S2.

## 135 **Data analysis**

### 136 *Statistical comparison*

137 Sample overlap was tested by computing the Jaccard distance (25) using the “vegan” R  
138 package and plotted into a heatmap using the “pheatmap” package (26). Clustering  
139 analysis was performed using the ‘Ward’ method. Principal component analysis was  
140 performed using the “stats” R package. Renyi entropy (27) was calculated using “vegan”  
141 and represents the distribution of clonal expansions as a function of the parameter *alpha*.  
142 Probability density plots were plotted using the “ggplot2” R package (28).

### 143 *Network analysis*

144 For each cell population, the following method was adopted: The top most frequent 1000  
145 CDR3 amino acid sequences from each of the six B6 or NOD mice were pooled and the



146 mean frequency was calculated for every sequence. The list was then ordered  
147 decreasingly and the first 1000 sequences were selected. A matrix of pairwise  
148 Levenshtein distances (LD) between the CDR3s was computed and used to construct the  
149 networks. In these networks, vertices (CDR3 sequences) are connected by edges (LD=1)  
150 only if they differ by one amino acid (insertion/deletion/substitution). A connected cluster  
151 is defined as a set of two or more vertices connected by edges. The clustering coefficient  
152 of a node in a network quantifies how close its neighbors are to being a clique (a closed  
153 cluster). The maximum value is 1 if every neighbor connected to the node A is also  
154 connected to every other node within the neighborhood. The node size represents the  
155 mean frequency of each CDR3 in the network.

156 Analyses were performed using R packages: “stringdist” (29) was used to calculate LDs  
157 and “Igraph” (30) to calculate network properties. Graphics visualization were done using  
158 Cytoscape (31) and “ggplot2” for figures 3 and 5 respectively. In the latter, only clustered  
159 nodes are represented and edges are not shown.

#### 160 *Identification of expanded clonotypes*

161 In each sample, the first (Q1) and third (Q3) quartiles and the interquartile range (IQR)  
162 were computed according to a negative binomial distribution fitted in the sequence read  
163 counts, while excluding private clonotypes with a count of 1. Expanded clonotypes are  
164 defined as those with counts greater than  $Q3 + 1.5 \times IQR$ .

#### 165 *TCR Database*

166 Mouse CDR3 $\beta$ s associated with diabetes (n=52), EAE (n=50), SLE (n=49) and cancer  
167 (n=52) were collected from Friedman’s published database (32). These sequences were  
168 derived from CD4<sup>+</sup> T cells and identified by different methods including reactivity

169 assays, tetramer staining, selection of diabetes-specific TCRs following diabetes  
170 induction and by sequencing of tumor T cell infiltrates in the context of cancer studies.

### 171 **Statistical analyses**

172 Statistical analyses were performed using the nonparametric Wilcoxon test with Holm  
173 multiple testing correction using “ggpubr” R package (33). A p value of  $\leq 0.05$  was  
174 considered statistically significant; \*  $p \leq 0.05$ , \*\*  $p \leq 0.01$ , \*\*\*  $p \leq 0.001$ , \*\*\*\*  $p \leq 0.0001$   
175 and n.s. denotes not significant ( $p > 0.05$ ). Mean percentage comparisons of diabetes,  
176 EAE, SLE and cancer CDR3s were done using the Wilcoxon paired test with diabetes as  
177 a reference group.

### 178 **Data availability**

179 Source data are provided in the manuscript and the Supplementary materials. Fastq data  
180 were deposited in NCBI Sequence Read Archive repository under the BioProject ID  
181 PRJNA635928.

182 **Results**

183 **Differences in repertoire composition between B6 and NOD**

184 We analyzed and compared the TCR beta chain (TRB) repertoire of splenic  
185 CD4<sup>+</sup>Foxp3<sup>+</sup>CD44<sup>low</sup>CD62L<sup>high</sup> nTregs, CD4<sup>+</sup>Foxp3<sup>+</sup>CD44<sup>high</sup> CD62L<sup>low</sup> amTregs and  
186 Foxp3<sup>-</sup>CD4<sup>+</sup> Teffs in B6 and NOD mice.

187 Compared to B6 mice, flow cytometry showed a significant decrease in the NOD Treg  
188 population ( $p \leq 0.05$ ) associated with a decrease of amTreg proportions ( $p \leq 0.01$ ) (Table  
189 S 1). Cell numbers for each sorted population and their corresponding number of TRB  
190 sequences and unique amino acid clonotypes are summarized in Table S2.

191 Principal component analysis of TRBVBJ usage, i.e. the frequency of each combination  
192 in the repertoire irrespective of the clonotype abundance, clearly separated the genetic  
193 backgrounds and the cell populations (Figure 1A). The first two components showed  
194 different TRBVBJ usage between B6 and NOD mice, with the first component (PC1) that  
195 separates the two genetic backgrounds explaining more than 68% of the variability. There  
196 was also a clear difference between the cell populations from the same background, with  
197 the two Treg subsets being close, but quite apart from Teffs. This reflects differences in  
198 the combined generation frequency and survival through the thymic selection and  
199 peripheral expansion of each generated TRBVBJ recombination.

200 To further investigate these differences, we assessed the clonotype (i.e. unique amino  
201 acid TRBV-CDR3-TRBJ sequence) overlap between samples using the Jaccard distance  
202 in which the higher the value, the more dissimilar the pair of samples compared (Figure  
203 1B). Hierarchical clustering on the Jaccard scores accurately separated B6 from NOD  
204 mouse samples. Surprisingly, within the latter cluster, amTregs are intermingled with  
205 nTregs and Teffs, while, as expected from our previous study (22), amTregs clustered

206 separately in the B6 background. Overall, NOD mice display a peculiar repertoire  
207 structure compared to B6 mice both at the TRB gene and clonotype level.

### 208 **Increased TCR diversity of Teffs and amTregs in NOD versus B6 mice**

209 We next explored the overall repertoire diversity at the clonotype level. We compared  
210 cell populations and mouse backgrounds by calculating the Renyi entropy, which  
211 evaluates diversity as a function of an *alpha* parameter (Figure 2A). The higher the *alpha*,  
212 the higher is the weight put on frequent clonotypes. The higher the Renyi entropy, the  
213 more diverse is the repertoire.

214 In B6 mice, nTregs have the most diverse repertoire while amTregs have the least diverse  
215 one, and Teffs fall in between. In contrast, while nTregs in NOD mice have a repertoire  
216 with a diversity similar to that in B6 mice, the diversities of the Teff and amTreg  
217 repertoires are increased compared to B6 mice (Figure 2A). At *alpha*=0, for which the  
218 Renyi index represents clonotype richness, no differences were observed between the B6  
219 and NOD backgrounds (Figure 2B, left). This indicates that the overall richness of each  
220 cell subset is not affected in NOD mice. At *alpha*=8, which gives more weight to  
221 abundant clonotypes, Renyi indices were significantly higher in NOD amTregs and Teffs  
222 than in the corresponding subsets in B6 mice (Figure 2B, right).

223 In view of these differences, we looked at the representativeness of the 100 most  
224 predominant clonotypes within each repertoire. The cumulative percentages of the 100  
225 most predominant clonotypes in B6 amTregs and Teffs were significantly higher than  
226 their NOD counterparts (Figure 2C). This is due to the presence, in the B6 cell  
227 populations, of highly frequent clonotypes depicted by blue lines which thickness is  
228 proportional to their percentage in the repertoire (Figure 2D). In contrast, there were no  
229 such clonotypes in B6 nor in NOD nTregs.

230 Collectively, these results reveal that a healthy naïve Treg repertoire is diverse with no  
231 clonotype expansions. Conversely, the healthy amTreg repertoire, and to a lesser extent  
232 the Teff repertoire, are enriched in clonotypes with high frequency, likely resulting from  
233 antigen-driven expansions. In diabetes-prone NOD mice, such expansions are severely  
234 reduced in amTregs and Teffs.

### 235 **Altered similarity structure of NOD amTreg and Teff repertoires**

236 Next, we examined the architecture of the repertoires. To this end, the 1000 most  
237 frequent CDR3s per population were used to build similarity networks in which each  
238 CDR3 (node) has a size proportional to its frequency and is connected by edges to other  
239 CDR3s that differ to it by only one amino acid, i.e. having a Levenshtein distance of 1  
240 (LD=1). This distance was shown to connect CDR3s that are likely to bind the same  
241 peptide (34).

242 The structure of the nTreg repertoire appeared similar for B6 and NOD mice, made of  
243 highly clustered CDR3s with low frequency (Figure 3A). In contrast, B6 amTreg  
244 repertoire was mostly composed of individual or lightly connected with high frequencies,  
245 reflecting polyclonal self-antigen-driven expansions (22,35). In accordance with the  
246 previous observations (Figures 1 and 2), these expansions are much reduced in amTregs  
247 from NOD mice. Similarly, node sizes of their Teffs appeared smaller than in B6 mice  
248 (Figure 3A, middle).

249 Node frequency showed no differences for nTregs, a modest decrease for Teffs and a  
250 marked decrease for amTregs in NOD mice compared to their counterparts in B6 mice  
251 (Figure 3B). The clustering coefficient of each CDR3 within each network, which gives  
252 an indication of the importance of these nodes in the global repertoire architecture,  
253 showed no significant difference between NOD and B6 nTregs (Figure 3C). However,

254 significantly higher clustering coefficients were observed in Teffs and amTregs from  
255 NOD compared to B6 mice.

256 Overall, the structural analysis of these networks highlights a higher sequence similarity  
257 of Teff and amTreg CDR3s in NOD mice. As IL-2 production is notoriously low in NOD  
258 mice and Tregs rely primarily on it for proliferation, we hypothesized that the reduced  
259 amTreg expansions may result from an IL-2 shortage.

### 260 **Low dose IL-2 normalizes NOD amTreg repertoires**

261 As administration of IL-2 to NOD mice specifically enables the expansion of Tregs (9),  
262 we investigated whether the abnormal repertoire diversity and structure of prediabetic  
263 NOD mice could be restored by an IL-2 treatment. NOD mice were injected with an  
264 adeno-associated virus coding for IL-2 (AAV-IL-2) that allows the continuous production  
265 of IL-2 at low dose and prevents the occurrence of diabetes (9). As expected, total Treg  
266 proportions increased significantly after IL-2 treatment (Figure 4A). Importantly, within  
267 the Treg subsets, amTreg proportions showed a significant increase, at the expense of  
268 nTregs (Figure 4A, Table S 3).

269 We next analyzed the expansions at the clonotype level after IL-2 treatment. To this end,  
270 we identified expanded clonotypes as the ones showing counts greater than the  
271  $Q3 + 1.5 \times IQR$  value, where Q3 is the third quartile and IQR the interquartile range of  
272 sequence count distribution (see the Methods section and Table S 4). The abundance of  
273 the expanded clonotypes from each sample was plotted in Figure 4B (left plots). Each  
274 circle represents a clonotype whose size is proportional to its frequency in the repertoire.  
275 amTregs and nTregs from AAV-IL-2-treated NOD mice were significantly enriched in  
276 expansions compared to amTregs and nTregs from B6 or NOD mice. This is confirmed  
277 by the density plots, which show that IL-2 treatment induces expansions of nTregs and

278 amTregs compared to their B6 and NOD counterparts, but not of Teffs (Figure 4B, right  
279 plot). Thus, IL-2 administration restores amTreg clonotype expansions that were absent  
280 in NOD mice.

### 281 **IL-2-expanded Tregs are enriched in diabetes-specific clonotypes**

282 We next examined whether the expanded clonotypes could be linked to diabetes. We  
283 queried a published catalogue of TCRs with defined specificity (32). We identified a total  
284 of 203 mouse CDR3 $\beta$  amino acid sequences from CD4<sup>+</sup> T cells associated with diabetes  
285 (n=52), experimental autoimmune encephalomyelitis (EAE; n=50), systemic lupus  
286 erythematosus (SLE; n=49) and cancer (n=52). We then searched for these sequences  
287 within the expanded clonotypes and calculated their mean enrichment in each cell subset  
288 (Figure 5A). Interestingly, diabetes-specific sequences showed higher expansions  
289 compared to non-diabetes-specific sequences in nTregs and amTregs from IL-2-treated  
290 NOD mice. There was also a modest enrichment of these sequences in B6 amTregs. To  
291 further analyze the specificity pattern towards diabetes, we connected disease-specific  
292 CDR3s by LD=1 to the pool of expanded amTreg and nTreg CDR3s. The number of  
293 neighbors with LD=1 to diabetes-related sequences showed a significant increase  
294 compared to other disease-specific CDR3s (Figure 5B).

295 Noteworthy, clonotypes identified as specific for islet antigens such as insulin and  
296 glutamic acid decarboxylase by tetramer staining were detected in large clusters of IL-2  
297 expanded clonotypes (Figure 5C, and Table S5).

### 298 **Discussion**

299 In this study, we report an altered amTreg TCR repertoire in NOD mice that can be  
300 restored to normal by an IL-2 treatment. IL-2 expanded Tregs were enriched in

301 islet-antigen-specific TCRs and were associated with protection from diabetes. These  
302 results have both heuristic and applied implications.

### 303 **The structure of the am- and n-Treg repertoires in a healthy mouse background**

304 In normal B6 mice, a control model that do not spontaneously develop any inflammatory  
305 or autoimmune diseases, nTreg repertoires are very diverse, even more than those of  
306 Teffs, with most clonotypes forming dense networks. These are the attributes of an  
307 unmodified and tightly connected post-thymic selection repertoire (36). In contrast,  
308 amTreg repertoires have a reduced diversity and are enriched in frequent clonotypes with  
309 few connections. This illustrates the responses to distinct self-antigens, as expected from  
310 a cell population that is constantly activated to control autoimmunity in numerous tissues.  
311 Such similarity structures have also been described in the context of immunization and  
312 aging (34).

313 In addition, amTreg repertoires show a higher overlap with each other than with nTregs  
314 or Teffs, indicating that the self-antigens to which amTregs respond are shared between  
315 individuals. This is also in agreement with our previous report of a low sequence overlap  
316 between the two Treg subsets in the peripheral lymph nodes (22). The comparison with  
317 Treg TRB repertoires from the NOD autoimmune-prone mouse strain strengthens this  
318 conclusion. Reduction of amTreg major expansions is associated with disease  
319 susceptibility, and their recovery with disease prevention.

320 Collectively, these results identify amTregs as the major subset involved in the  
321 pathogenesis of autoimmunity and warrant separate analysis of amTregs and nTregs  
322 when investigating their roles in health or disease.

### 323 **amTreg activation depends on IL-2**



324 The severe reduction in frequent clonotypes found in NOD mice, and their appearance  
325 under IL-2 provision, highlight a major role of IL-2 in supporting amTreg survival.  
326 NOD mice have a genetically determined IL-2 insufficiency, which is also reported in  
327 human type 1 diabetes as well as in SLE and rheumatoid arthritis (37,38). It is thus likely  
328 that the observed defect in amTreg fitness contributes to the pathophysiology of these  
329 diseases. If so, the good news is that disease-relevant amTregs can be regenerated by IL-  
330 2 treatment. We show herein that one injection of rAAV-IL-2 in prediabetic mice was  
331 enough to expand NOD amTregs at the cell and repertoire levels. In our experiments, the  
332 repertoire was analyzed 21 days after the initiation of treatment. As the approximate  
333 duration of T cell differentiation in the thymus is of 28 days (39), newly generated  
334 thymocytes are unlikely to contribute to the expanded clonotypes in the amTreg  
335 population. Thus, the IL-2-induced amTregs most probably originate from peripheral  
336 amTregs and/or nTregs that received their activation signal in the presence of IL-2. The  
337 diabetes-related TCR expansions in both nTregs and amTregs further support that both  
338 populations contribute to the restoration of a more balanced and complete disease-  
339 relevant amTreg repertoire.

#### 340 **Treg specificity to diabetes-related antigens**

341 The existence of public databases containing TCRs with known peptide specificities  
342 allowed us to investigate the presence of antigen-specific sequences in our repertoires.  
343 Diabetes-related CDR3s identified from the database were overrepresented in IL-  
344 2-treated NOD Tregs and most connected in LD=1 networks, as shown by their high  
345 number of neighbors. Linking the CDR3 similarity networks to annotated TCR datasets  
346 was previously described by Madi et al., and showed that CDR3s with similar specificity

347 tend to cluster together (34). This indicates that diabetes-specific CDR3s could have core  
348 motifs engaged in pancreatic antigen recognition, and shows the potential of such a tool  
349 in identifying novel pathogenic TCRs. Indeed, repertoire analysis of islet-infiltrating T  
350 cells revealed an accumulation of TCRs that were reactive in vitro to uncharacterized  
351 autoantigens, distinct from the well-known glutamic acid decarboxylase and insulin  
352 antigens (13).

353 These observations highlight a relationship between the specific expansion of pancreatic  
354 antigen-related TCRs and the prevention of diabetes post IL-2 treatment.

### 355 **Contribution of I-A<sup>g7</sup> to NOD pathophysiology**

356 It was hypothesized that diabetes development in NOD mice is associated with the  
357 I-A<sup>g7</sup> molecule that they express. Co-expression with a different type of MHC or  
358 mutations within the I-A<sup>g7</sup> molecule were shown to prevent insulinitis and diabetes (4, 40).

359 On the other hand, substitution of non-MHC regions from the C57BL/10 into the NOD  
360 strain was sufficient to prevent insulinitis or diabetes, despite their expression of the I-A<sup>g7</sup>  
361 molecule (41). Our studies highlight the importance of non-MHC genes in diabetes onset  
362 in the NOD mouse model. Indeed, we report here that IL-2 administration to pre-diabetic  
363 NOD mice, previously shown to prevent the disease outcome, improves amTreg fitness.  
364 This would argue that NOD Treg repertoires have the full potential to control  
365 autoimmune responses, but fail to do so because an IL-2 deficiency impairs the amTreg  
366 repertoire that can control islet autoreactivity.

367 However, our results do not exclude a potential enrichment of autoreactive T cells in the  
368 NOD mice repertoire that would take the lead in the periphery where Tregs fail to  
369 expand. In this regard, NOD mice have an overrepresentation of CDR3 $\beta$  sequences

370 carrying hydrophobic amino acid doublets at positions 6 and 7 that have been shown to  
371 confer high self-reactivity (42). Further studies of the TCR repertoire selection process in  
372 the thymus of NOD mice should help address this important issue.

373 Altogether, our results reveal a link between a reduced expansion of clonotypes within  
374 the activated Treg TCR repertoire and the development of an autoimmune disease.-IL-2  
375 treatment not only activates Tregs, but also restores a repertoire of TCRs with relevant  
376 specificities. Thus, our work indicates that fit amTregs are key to protection from  
377 autoimmune diseases and highlights the value of studying these cells separately from the  
378 whole Treg population. Importantly, amTreg repertoire abnormalities and restoration are  
379 detected in the spleen, which affords a readout that is more representative of the  
380 circulation than pancreatic lymph nodes and thus has a translational value. Our results  
381 should guide further studies to elucidate the dynamics of pancreatic antigen-specific  
382 amTregs in diabetic versus non-diabetic NOD mice, including in mice outside of a  
383 pathogen-free environment, and identify TCR-based biomarkers of diabetes.

384

385 **Acknowledgments**

386 We thank F. Jebbawi and L. Barientos for their help in sample collection and cell sorting,  
387 M. Mendez and N. Papaya for their help in RNA extraction and library preparations, and  
388 K. El Soufi for his help in network analyses. We thank the staff of the animal care facility  
389 for their excellent handling of mice. We also thank the UMR 8199 LIGAN-PM  
390 Genomics platform (Lille, France) which belongs to the ‘Federation de Recherche’ 3508  
391 Labex EGID (European Genomics Institute for Diabetes; ANR-10-LABX-46) and was  
392 supported by the ANR Equipex 2010 session, for performing the sequencing of our  
393 libraries.

394 **Funding**

395 This work was funded by the TRiPoD ERC-Advanced EU (No. 322856) and RHU iMAP  
396 (ANR-16-RHUS-0001) grants to DK, with additional support from the Sorbonne  
397 Université, INSERM and AP-HP. ILTOO pharma supported HPP.

398 **Author contributions**

399 VM, GF, PB, VQ, GC, FB, BG, P-GR and EM-F performed the experiments. VM  
400 analyzed the data, with contributions from all authors. VM and HPP performed the  
401 statistical analyses. VM, EM-F, AS and DK conceived the experiments. VM, AS, EM-F  
402 and DK wrote the manuscript, with input from all authors. DK conceptualized and  
403 supervised the study and is the guarantor for the contents of the article.

404 **Duality of interest**

405 DK is an investor of a patent related to the use of IL-2 in the treatment of autoimmune  
406 diseases, owned by his public institution and licensed to ILTOO pharma, in which DK  
407 has interests. The other authors declare no competing financial interests.

408

409 **References**

410 1. J. Verdaguer, D. Schmidt, A. Amrani, B. Anderson, N. Averill, P. Santamaria,  
411 Spontaneous autoimmune diabetes in monoclonal T cell nonobese diabetic mice. *J. Exp.*  
412 *Med.* **186**, 1663–1676 (1997).

413 2. Y.-G. Chen, C. E. Mathews, J. P. Driver, The Role of NOD Mice in Type 1 Diabetes  
414 Research: Lessons from the Past and Recommendations for the Future. *Front.*  
415 *Endocrinol.* **9**, 51 (2018).

416 3. O. Kanagawa, B. A. Vaupel, G. Xu, E. R. Unanue, J. D. Katz, Thymic positive  
417 selection and peripheral activation of islet antigen-specific T cells: separation of two  
418 diabetogenic steps by an I-A(g7) class II MHC beta-chain mutant. *J. Immunol.* **161**,  
419 4489–4492 (1998).

420 4. T. Lund, L. O'Reilly, P. Hutchings, O. Kanagawa, E. Simpson, R. Gravely, P.  
421 Chandler, J. Dyson, J. K. Picard, A. Edwards, D. Kioussis, A. Cooke, Prevention of  
422 insulin-dependent diabetes mellitus in non-obese diabetic mice by transgenes encoding  
423 modified I-A  $\beta$ -chain or normal I-E  $\alpha$ -chain. *Nature.* **345**, 727–729 (1990).

424 5. D. Klatzmann, A. K. Abbas, The promise of low-dose interleukin-2 therapy for  
425 autoimmune and inflammatory diseases. *Nature Reviews Immunology.* **15**, 283–294  
426 (2015).

427 6. S. A. Long, K. Cerosaletti, P. L. Bollyky, M. Tatum, H. Shilling, S. Zhang, Z.-Y.  
428 Zhang, C. Pihoker, S. Sanda, C. Greenbaum, J. H. Buckner, Defects in IL-2R signaling  
429 contribute to diminished maintenance of FOXP3 expression in CD4(+)CD25(+)  
430 regulatory T-cells of type 1 diabetic subjects. *Diabetes.* **59**, 407–415 (2010).

431 7. E. Sgouroudis, A. Albanese, C. A. Piccirillo, Impact of protective IL-2 allelic variants  
432 on CD4+ Foxp3+ regulatory T cell function in situ and resistance to autoimmune diabetes  
433 in NOD mice. *J. Immunol.* **181**, 6283–6292 (2008).

434 8. C. J. Dwyer, A. L. Bayer, C. Fotino, L. Yu, C. Cabello-Kindelan, N. C. Ward, K. H.  
435 Toomer, Z. Chen, T. R. Malek, Altered homeostasis and development of regulatory T cell  
436 subsets represent an IL-2R-dependent risk for diabetes in NOD mice. *Sci Signal.* **10**  
437 (2017), doi:10.1126/scisignal.aam9563.

438 9. G. Churlaud, V. Jimenez, J. Ruberte, M. Amadoudji Zin, G. Fourcade, G. Gottrand, E.  
439 Casana, B. Lambrecht, B. Bellier, E. Piaggio, F. Bosch, D. Klatzmann, Sustained  
440 stimulation and expansion of Tregs by IL2 control autoimmunity without impairing  
441 immune responses to infection, vaccination and cancer. *Clinical Immunology.* **151**, 114–  
442 126 (2014).

443 10. M. Rosenzweig, G. Churlaud, R. Mallone, A. Six, N. Dérian, W. Chaara, R.  
444 Lorenzon, S. A. Long, J. H. Buckner, G. Afonso, H.-P. Pham, A. Hartemann, A. Yu, A.  
445 Pugliese, T. R. Malek, D. Klatzmann, Low-dose interleukin-2 fosters a dose-dependent

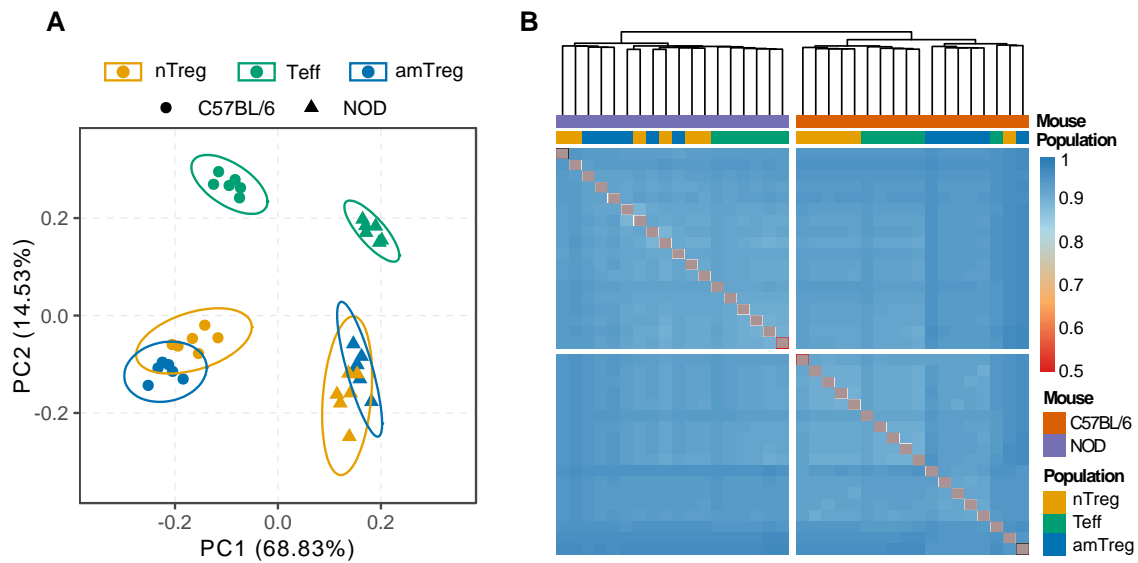
- 446 regulatory T cell tuned milieu in T1D patients. *Journal of Autoimmunity*. **58**, 48–58  
447 (2015).
- 448 11. I. Marrero, A. Vong, Y. Dai, J. D. Davies, T cell populations in the pancreatic lymph  
449 node naturally and consistently expand and contract in NOD mice as disease progresses.  
450 *Molecular Immunology*. **52**, 9–18 (2012).
- 451 12. L. Li, Q. He, A. Garland, Z. Yi, L. T. Aybar, T. B. Kepler, J. A. Frelinger, B. Wang,  
452 R. Tisch, Cell-Specific CD4<sup>+</sup> T Cell Clonotypes in Peripheral Blood and the Pancreatic  
453 Islets Are Distinct. *The Journal of Immunology*. **183**, 7585–7591 (2009).
- 454 13. F. J. Baker, M. Lee, Y. -h. Chien, M. M. Davis, Restricted islet-cell reactive T cell  
455 repertoire of early pancreatic islet infiltrates in NOD mice. *Proceedings of the National  
456 Academy of Sciences*. **99**, 9374–9379 (2002).
- 457 14. Nakano, T cell receptor V gene usage of islet beta cell-reactive T cells is not  
458 restricted in non-obese diabetic mice. *Journal of Experimental Medicine*. **173**, 1091–1097  
459 (1991).
- 460 15. I. Marrero, D. E. Hamm, J. D. Davies, High-Throughput Sequencing of Islet-  
461 Infiltrating Memory CD4<sup>+</sup> T Cells Reveals a Similar Pattern of TCR V $\beta$  Usage in  
462 Prediabetic and Diabetic NOD Mice. *PLoS ONE*. **8**, e76546 (2013).
- 463 16. I. Marrero, C. Aguilera, D. E. Hamm, A. Quinn, V. Kumar, High-throughput  
464 sequencing reveals restricted TCR V $\beta$  usage and public TCR $\beta$  clonotypes among  
465 pancreatic lymph node memory CD4<sup>+</sup> T cells and their involvement in autoimmune  
466 diabetes. *Molecular Immunology*. **74**, 82–95 (2016).
- 467 17. H. R. Seay, E. Yusko, S. J. Rothweiler, L. Zhang, A. L. Posgai, M. Campbell-  
468 Thompson, M. Vignali, R. O. Emerson, J. S. Kaddis, D. Ko, M. Nakayama, M. J. Smith,  
469 J. C. Cambier, A. Pugliese, M. A. Atkinson, H. S. Robins, T. M. Brusko, Tissue  
470 distribution and clonal diversity of the T and B cell repertoire in type 1 diabetes  
471 (2016),doi:10.1172/jci.insight.88242.
- 472 18. C. Ferreira, Y. Singh, A. L. Furmanski, F. S. Wong, O. A. Garden, J. Dyson, Non-  
473 obese diabetic mice select a low-diversity repertoire of natural regulatory T cells.  
474 *Proceedings of the National Academy of Sciences*. **106**, 8320–8325 (2009).
- 475 19. J. Kern, R. Drutel, S. Leanhart, M. Bogacz, R. Pacholczyk, Reduction of T Cell  
476 Receptor Diversity in NOD Mice Prevents Development of Type 1 Diabetes but Not  
477 Sjögren's Syndrome. *PLoS ONE*. **9**, e112467 (2014).
- 478 20. P.-G. Ritvo, A. Saadawi, P. Barennes, V. Quiniou, W. Chacara, K. El Soufi, B.  
479 Bonnet, A. Six, M. Shugay, E. Mariotti-Ferrandiz, D. Klatzmann, High-resolution  
480 repertoire analysis reveals a major bystander activation of Tfh and Tfr cells. *Proc Natl  
481 Acad Sci USA*. **115**, 9604–9609 (2018).

- 482 21. S. Fisson, G. Darrasse-Jèze, E. Litvinova, F. Septier, D. Klatzmann, R. Liblau, B. L.  
483 Salomon, Continuous activation of autoreactive CD4<sup>+</sup> CD25<sup>+</sup> regulatory T cells in the  
484 steady state. *J. Exp. Med.* **198**, 737–746 (2003).
- 485 22. A.-S. Bergot, W. Chaara, E. Ruggiero, E. Mariotti-Ferrandiz, S. Dulauroy, M.  
486 Schmidt, C. von Kalle, A. Six, D. Klatzmann, TCR sequences and tissue distribution  
487 discriminate the subsets of naïve and activated/memory Treg cells in mice: Molecular  
488 immunology. *European Journal of Immunology.* **45**, 1524–1534 (2015).
- 489 23. P. Barennes, V. Quiniou, M. Shugay, E. S. Egorov, A. N. Davydov, D. M. Chudakov,  
490 I. Uddin, M. Ismail, T. Oakes, B. Chain, A. Eugster, K. Kashofer, P. P. Rainer, S. Darko,  
491 A. Ransier, D. C. Douek, D. Klatzmann, E. Mariotti-Ferrandiz, Benchmarking of T cell  
492 receptor repertoire profiling methods reveals large systematic biases. *Nat Biotechnol*  
493 (2020)
- 494 24. D. A. Bolotin, S. Poslavsky, I. Mitrophanov, M. Shugay, I. Z. Mamedov, E. V.  
495 Putintseva, D. M. Chudakov, MiXCR: software for comprehensive adaptive immunity  
496 profiling. *Nature Methods.* **12**, 380–381 (2015).
- 497 25. P. Jaccard, Étude comparative de la distribution florale dans une portion des Alpes et  
498 du Jura. *Imprimerie Corbaz & Comp.* (1901)
- 499 26. R. Kolde, pheatmap (2019).
- 500 27. R. Alfred, On measures of entropy and information. In: *Proceedings of the Fourth*  
501 *Berkeley Symposium on Mathematical Statistics and Probability* (1961), pp. 547–61.
- 502 28. H. Wickham, D. Navarro, T. Lin Pedersen, *ggplot2: Elegant Graphics for Data*  
503 *Analysis* (Springer, 2nd edition).
- 504 29. P.J. van der Loo, Mark, The stringdist Package for ApproximateString Matching. *The*  
505 *R Journal.* Vol. 6/1, (2020)
- 506 30. G. Csardi, T. Nepusz, The igraph software package for complex network research  
507 (2006).
- 508 31. P. Shannon, Cytoscape: A Software Environment for Integrated Models of  
509 Biomolecular Interaction Networks. *Genome Research.* **13**, 2498–2504 (2003).
- 510 32. N. Tickotsky, T. Sagiv, J. Prilusky, E. Shifrut, N. Friedman, McPAS-TCR: a  
511 manually curated catalogue of pathology-associated T cell receptor sequences.  
512 *Bioinformatics.* **33**, 2924–2929 (2017).
- 513 33. Alboukadel, ggpubr R Package: ggplot2-Based Publication Ready Plots (2020)
- 514 34. A. Madi, A. Poran, E. Shifrut, S. Reich-Zeliger, E. Greenstein, I. Zaretsky, T. Arnon,  
515 F. V. Laethem, A. Singer, J. Lu, P. D. Sun, I. R. Cohen, N. Friedman, T cell receptor  
516 repertoires of mice and humans are clustered in similarity networks around conserved  
517 public CDR3 sequences. *eLife.* **6** (2017), doi:10.7554/eLife.22057.

- 518 35. G. Darrasse-Jèze, A.-S. Bergot, A. Durgeau, F. Billiard, B. L. Salomon, J. L. Cohen,  
519 B. Bellier, K. Podsypanina, D. Klatzmann, Tumor emergence is sensed by self-specific  
520 CD44<sup>hi</sup> memory Tregs that create a dominant tolerogenic environment for tumors in  
521 mice. *Journal of Clinical Investigation* (2009)
- 522 36. Y. Elhanati, A. Murugan, C. G. Callan, T. Mora, A. M. Walczak, Quantifying  
523 selection in immune receptor repertoires. *Proceedings of the National Academy of*  
524 *Sciences*. **111**, 9875–9880 (2014).
- 525 37. G. D. Kitas, M. Salmon, M. Farr, J. S. Gaston, P. A. Bacon, Deficient interleukin 2  
526 production in rheumatoid arthritis: association with active disease and systemic  
527 complications. *Clin. Exp. Immunol.* **73**, 242–249 (1988).
- 528 38. K. S. Zier, M. M. Leo, R. S. Spielman, L. Baker, Decreased Synthesis of Interleukin-  
529 2 (IL-2) in Insulin-dependent Diabetes Mellitus. *Diabetes*. **33**, 552–555 (1984).
- 530 39. V. Thomas-Vaslin, H. K. Altes, R. J. de Boer, D. Klatzmann, Comprehensive  
531 Assessment and Mathematical Modeling of T Cell Population Dynamics and  
532 Homeostasis. *J Immunol.* **180**, 2240–2250 (2008).
- 533 40. L. Gioia, M. Holt, A. Costanzo, S. Sharma, B. Abe, L. Kain, M. Nakayama, X. Wan,  
534 A. Su, C. Mathews, Y.-G. Chen, E. Unanue, L. Teyton, Position  $\beta$ 57 of I-A<sup>g7</sup> controls  
535 early anti-insulin responses in NOD mice, linking an MHC susceptibility allele to type 1  
536 diabetes onset. *Sci. Immunol.* **4**, eaaw6329 (2019).
- 537 41. D. V. Serreze, M. Bridgett, H. D. Chapman, E. Chen, S. D. Richard, E. H. Leiter,  
538 Subcongenic Analysis of the Idd13 Locus in NOD/Lt Mice: Evidence for Several  
539 Susceptibility Genes Including a Possible Diabetogenic Role for  $\beta$ 2-Microglobulin. *The*  
540 *Journal of Immunology*. **160**, 1472–1478 (1998).
- 541 42. B. D. Stadinski, K. Shekhar, I. Gómez-Touriño, J. Jung, K. Sasaki, A. K. Sewell, M.  
542 Peakman, A. K. Chakraborty, E. S. Huseby, Hydrophobic CDR3 residues promote the  
543 development of self-reactive T cells. *Nature Immunology*. **17**, 946–955 (2016).
- 544



545 **Figures**



546

547

548 **Figure 1. B6 and NOD mice express different TCR repertoires. (A)** PCA biplot for

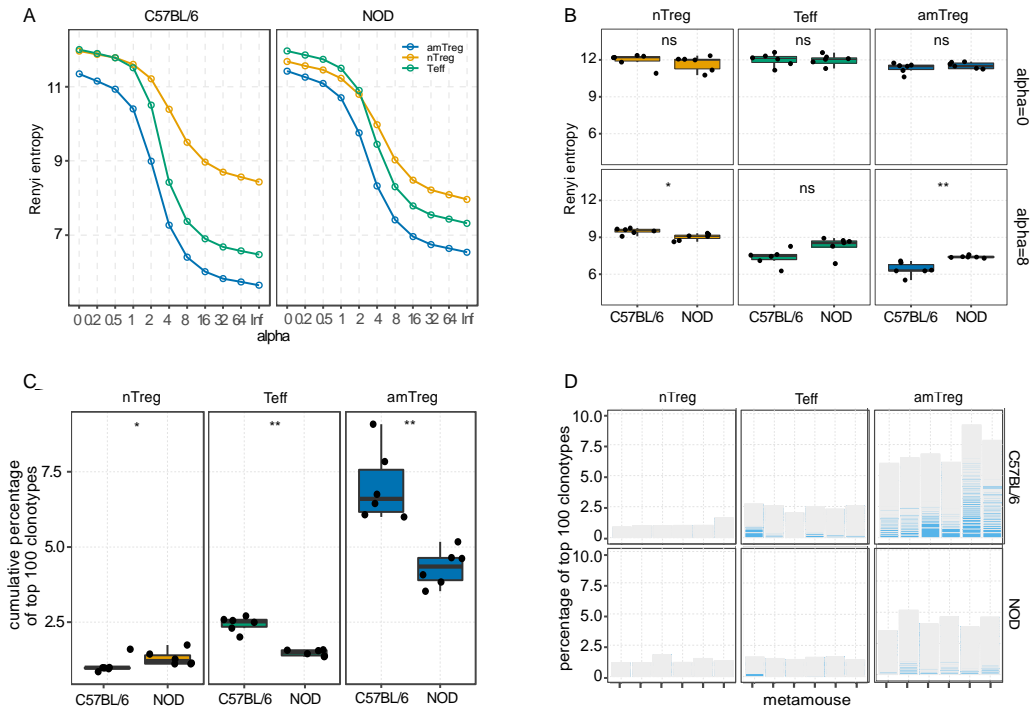
549 TRBVBJ usage of all B6 (dots) and NOD (triangles) samples. Cell populations are

550 identified based on their colors. **(B)** Heatmap of the pairwise Jaccard distances calculated

551 at the clonotype level. Scores range between 0 (complete similarity) and 1 (no similarity).

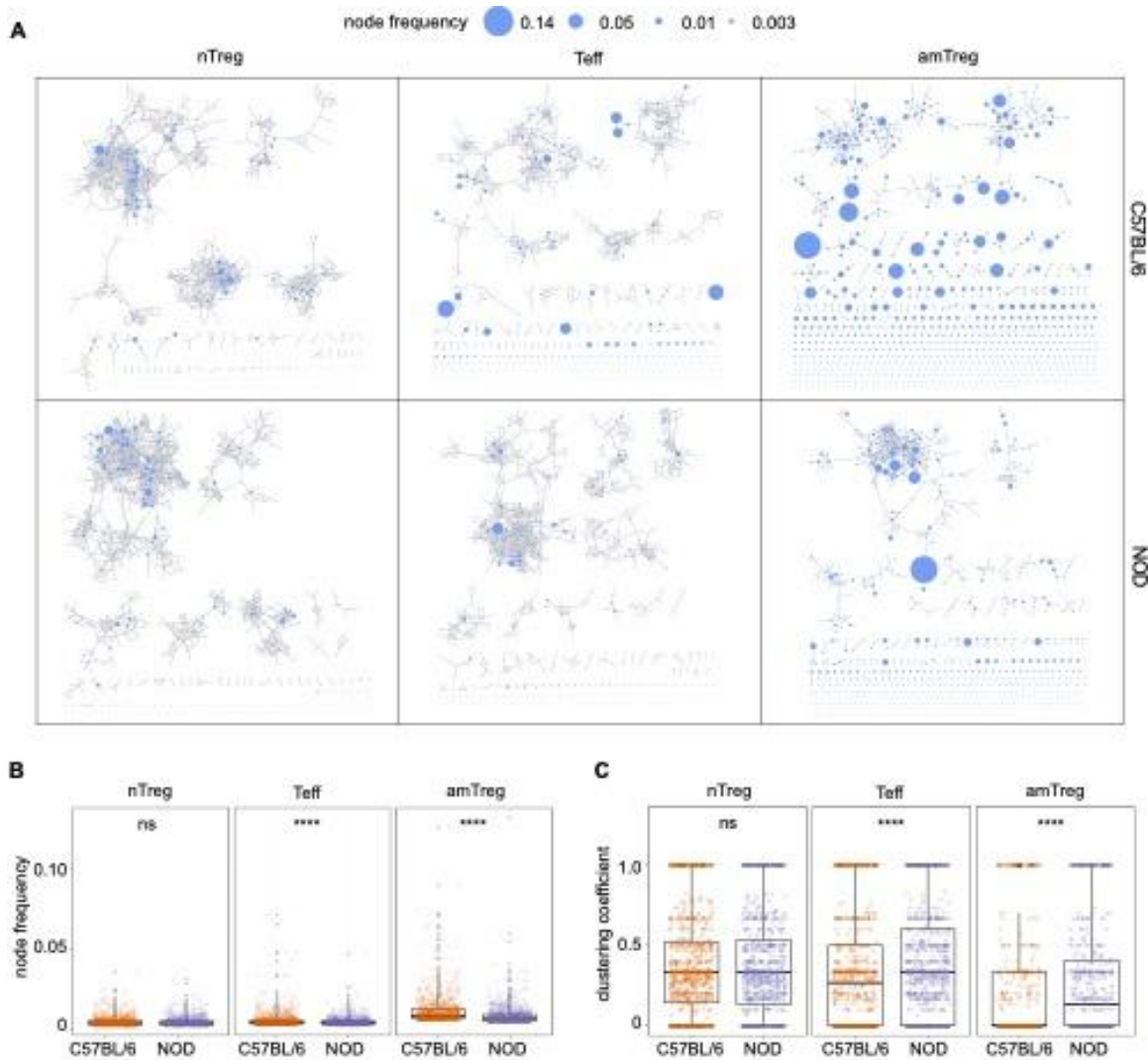
552 The hierarchical clustering was performed using Ward's method.

553



554

555 **Figure 2. Increased diversity of NOD Teffs and amTregs compared to B6.** (A) Renyi  
 556 profiles for nTregs (yellow), CD4 Teffs (green) and amTregs (blue) in B6 and NOD  
 557 mice. Points represent the mean of all six mice and shaded areas represent the standard  
 558 error. (B) Renyi values were compared between B6 and NOD mice within each cell  
 559 population at  $\alpha = 0$  and  $\alpha = 8$ . (C) Mean cumulative percentage of the 100 most  
 560 predominant clonotypes of the six mice for each cell population. (D) Percentage of the  
 561 top 100 clonotypes within the three cell populations in B6 (upper plot) and in NOD  
 562 (lower plot) backgrounds. Each blue line and its thickness represent a unique clonotype  
 563 and its occurrence, grey “bars” are the stacking of slim grey lines representing rare  
 564 clonotypes. (B, C)  $n=6$ , ns  $P > 0.05$ , \*  $P \leq 0.05$ , \*\*  $P \leq 0.01$ , Wilcoxon test with Holm’s  
 565 correction.



567

568

**Figure 3. Similarity structure of nTreg, Teff and amTreg CDR3 repertoires.** (A) For

569

each cell population, the most frequent 1000 CDR3s across all mice were identified based

570

on their mean frequency and used to construct networks based on the Levenshtein

571

distance: CDR3 sequences (nodes) with one amino acid difference

572

(insertion/deletion/substitution) are connected by an edge. One network was constructed

573

per cell population and mouse background. (B) CDR3 frequency comparison between B6

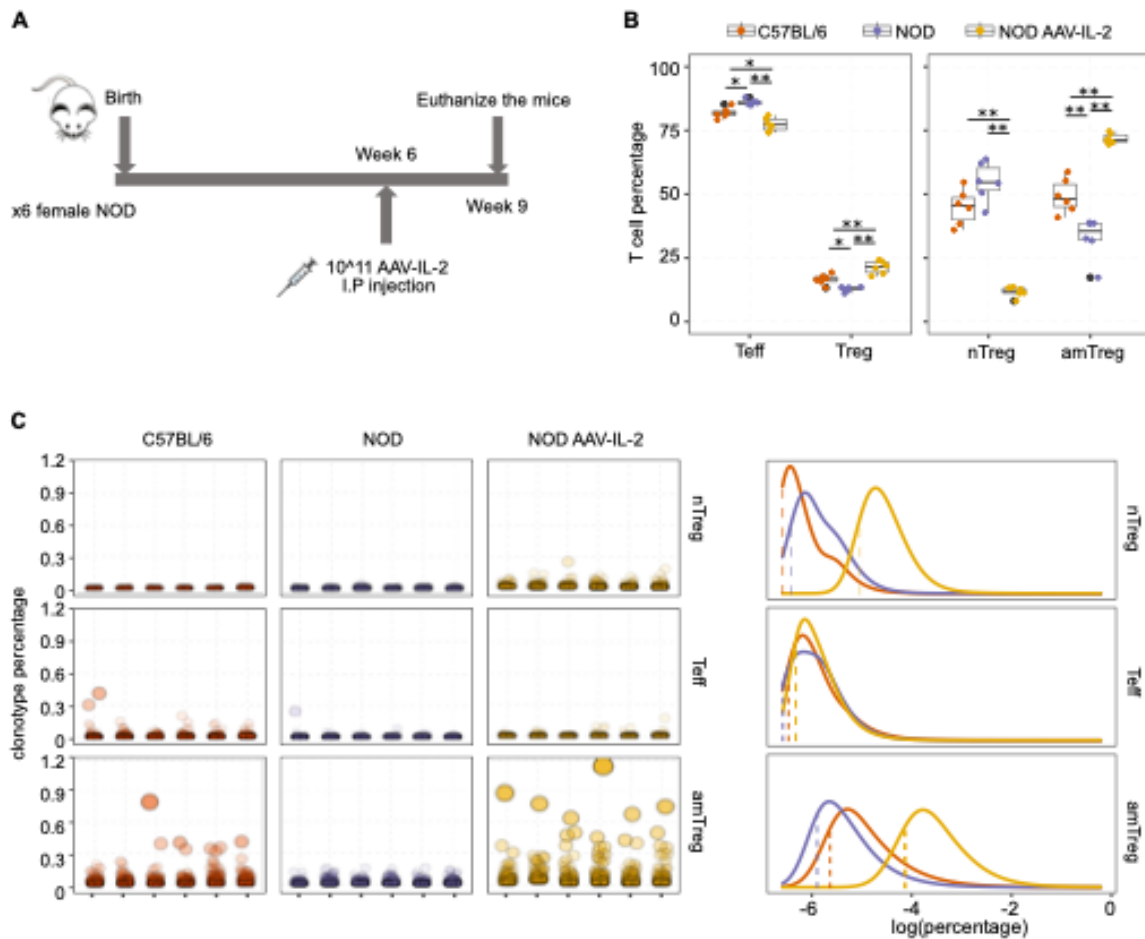
574

and NOD mice for each cell subset. (C) Comparison of the-clustering coefficient, which

575

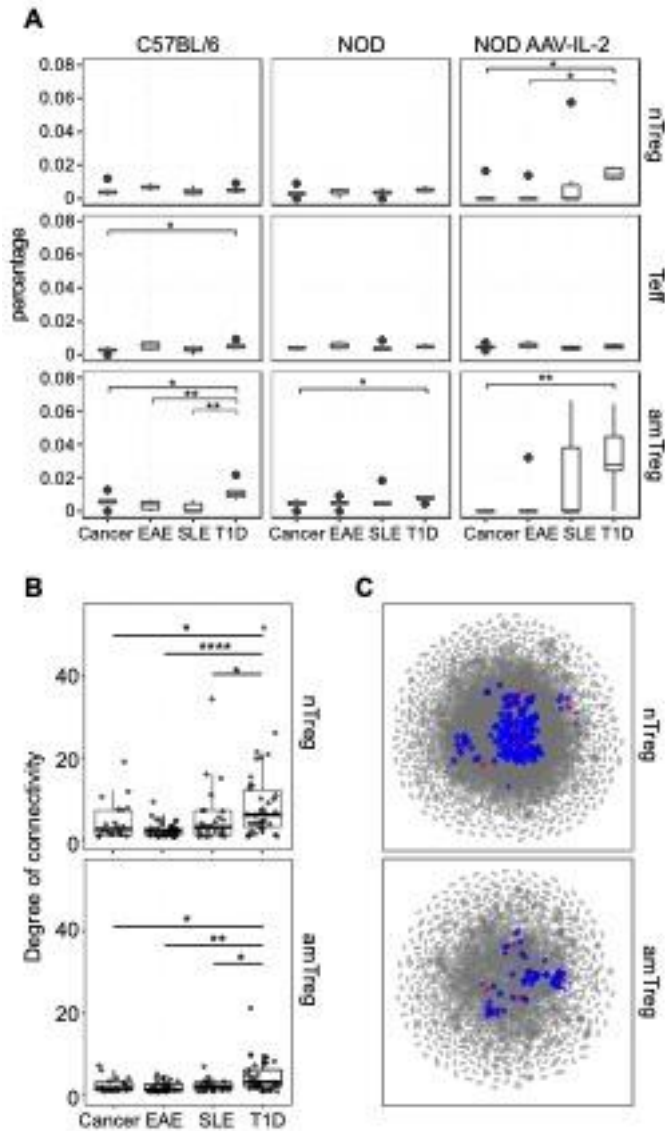
quantifies the degree to which neighbor nodes tend to cluster together, between B6 and

576 NOD mice in each cell subset. CDR3s with no connections are excluded. **(B, C)** Each dot  
 577 represents a CDR3 and boxplots represent the median, first and third quartiles. ns  $P >$   
 578 0.05, \*\*\*  $P \leq 0.001$ , \*\*\*\*  $P \leq 0.0001$ , Wilcoxon test with Holm's correction.



579 **Figure 4. IL-2 induces Treg clonotype expansions.** (A) Experimental scheme. (B) Box  
 580 plots show the percentage of T cells in each B6 (orange), NOD (purple) and IL-2–treated  
 581 NOD (yellow) mice (n=6 per background). (C, left plot) The abundance (in %) of  
 582 expanded clonotypes for each sample (each column represents a single sample) within the  
 583 three populations and mouse backgrounds. Expanded clonotypes were identified as the  
 584 ones with counts greater than  $Q3 + 1.5 \times IQR$  according to a fitted negative binomial  
 585

586 distribution. **(C, right plot)** Probability density plot based on the mean expanded  
 587 clonotype distribution between the three mouse conditions for each cell subset. Colored  
 588 dashed lines represent the mode of each curve.



589 **Figure 5. IL-2 preferentially expands clonotypes with a diabetes-related specificity.**  
 590 **(A)** The proportion of CDR3s specific for cancer, EAE, SLE and diabetes found within  
 591 the expanded clonotypes of each population (n=6). Box-and-whisker plots show the  
 592 median and outliers. **(B)** CDR3s with a disease-related specificity were connected by  
 593

594 LD=1 to the pool of amTreg and nTreg CDR3s identified across the six IL-2 treated  
595 NOD mice. The degree of connectivity, i.e the number of LD=1 edges connecting a given  
596 node, of disease-specific CDR3s is plotted (n=52 in cancer, n=50 in EAE, n=49 in SLE  
597 and n=52 in T1D). **(A, B)** Wilcoxon test was performed with the T1D group as a  
598 reference: ns  $p > 0.05$ , \*  $P \leq 0.05$ , \*\*  $P \leq 0.01$  and \*\*\*  $P \leq 0.001$ . **(C)** Graphical  
599 representation of the LD=1 networks in NOD AAV-IL-2 treated nTregs and amTregs.  
600 Unconnected sequences are not shown. Identical sequences found in the database and  
601 samples from IL-2 treated mice are shown in red, their neighbors in blue as well as  
602 diabetes-related sequences from the database.